Dynamics of Magnetization in Hyperpolarized Gas MRI of the Lung

G. Allan Johnson, Gordon Cates, X. Josette Chen, Gary P. Cofer, Bastiaan Driehuys, Will Happer, Laurence W. Hedlund, Brian Saam, Mark D. Shattuck, John Swartz

The magnetization in hyperpolarized gas (HP) MRI is generated by laser polarization that is independent of the magnet and imaging process. As a consequence, there is no equilibrium magnetization during the image acquisition. The competing processes of gas inflow and depolarization of the spins lead to large changes in signal as one samples k-space. A model is developed of dynamic changes in polarization of hyperpolarized ^{3}He during infusion and in vivo imaging of the lung and verified experimentally in a live guinea pig. Projection encoding is used to measure the view-to-view variation with temporal resolution <4 ms. Large excitation angles effectively sample the magnetization in the early stages of inflow, highlighting larger airways, while smaller excitation angles produce images of the more distal spaces. The work provides a basis for pulse sequences designed to effectively exploit HP MRI in the lung.

Key words: hyperpolarized gas; lung; guinea pig.

INTRODUCTION

The recent demonstration of MR images using hyperpolarized (HP) gas has generated particular promise in the lung (1–5). The low proton density, as well as the short T_2 and T_2^* of lung, make imaging with conventional ^{1}H MRI particularly challenging. Middleton et al. estimate the improvement in signal-to-noise (SNR) of 30% polarized ^{3}He to be 10 times greater than an equal volume of water imaged at 2.0 Tesla (1). Because the proton density of lung is ~0.10 g/cc, this translates to as much as a 100-fold improvement in SNR for lung imaging. Moreover, since one is directly imaging the gas in the air spaces of the lung, HP MRI may provide a direct measure of lung function.

Several excellent papers have focused on polarization changes arising from relaxation and transport of ^{129}Xe (6, 7), but little work has been directed at the dynamics of depolarization associated with a given imaging tech-nique. Work has focused instead on the essentials of gas production and delivery, and the fundamental physical properties of the gas. Refinement of the gas production apparatus has advanced to the point that we are now able to routinely produce ~350 cc of gas polarized to 5–10% in ~8 h. Thus, it becomes possible to systematically explore the time course of magnetization in an HP MRI study, which is crucial to fully exploit this powerful new imaging method.

In conventional MRI, the population difference between energy levels is due to the interaction of the nuclear magnetization with the externally applied field (B_0). In HP MRI, the sample is prepolarized; hence, the extent of the polarization is independent of the field strength of the imaging system. There are two consequences: a) there is no recovery of magnetization between individual views, and b) there will be significant variation in the magnetization during the course of a breath. When imaging the lung, we assume an input bolus of magnetization, that is, a point in time when there is no signal source followed by some time course during which the gas flows into the lung. One might reasonably expect an initial magnetization of zero, followed by a large increase in magnetization over a short period as gas flows into the lung, followed by another period during which the magnetization is destroyed by the imaging process. Ideally, one would like to sample the magnetization as effectively as possible so that hard won signal is not "exhaled."

Upon reflection on the time course of the magnetization, a number of additional questions not encountered in traditional proton MRI arise. For example, the magnetization must clearly vary a great deal from view to view; how much variation might we expect? What are the consequences in choosing imaging strategies, e.g., Cartesian versus radial trajectories? What are the consequences of the timing and RF excitation on the "contrast" in the images? One is faced with two conflicting goals: a) to optimize the use of the polarization, and b) to minimize the artifacts arising from variation in the magnetization over the imaging period. The goal of this research is to understand the dynamics of the magnetization in HP MRI of the lung. By so doing, we hope to lay the groundwork for a number of new strategies to optimize imaging with HP gas.

THEORY

We consider the simplest possible imaging strategy, that is, the acquisition of a free induction decay (FID) with projection encoding. The signal generated in a FID with

excitation angle, α, from an initial magnetization, M_0, is given in Eq. [1]:

$$S = M_0 \sin \alpha \qquad [1]$$

The residual magnetization, $M_r(i)$, after the ith RF excitation, is related to the previous residual magnetization, $M_r(i - 1)$, by Eq. [2]:

$$M_r(i) = M_r(i - 1) \cos \alpha \qquad [2]$$

It is straightforward to demonstrate that the signal $S(i)$ in the ith FID is

$$S(i) = M_0 \sin \alpha \cos^i \alpha \qquad [3]$$

We have ignored T_1 decay based on our previous studies (1) in which there was substantial signal in the lung of a dead guinea pig after 3.5 min. The model is limited to a single ventilatory cycle of <2 s. For longer acquisition times, T_1 decay in the reservoir must be included, but this is a simple exponential decay imposed on the input magnetization. We have modeled the infusion of gas into the lung as a series of j square pulses representing boluses of helium input into the lung over j ventilatory cycles. The new magnetization arising from the bolus in the ith view of the jth ventilatory cycle is $M_n(i, j)$. The boluses are diluted by the functional residual capacity so that at the end of each ventilatory cycle, a fraction of the residual magnetization is lost as it is exhaled. In our experiments, the ^{3}He breaths are interleaved with breaths of air/isoflurane required to keep the animal anesthetized and appropriately ventilated. There is additional signal loss from T_1 decay during these interleaved cycles when no views are acquired. Thus the residual magnetization in the first view of the jth ventilatory cycle is diminished by a factor f, representing losses from exhalation and T_1 decay, that is,

$$M_r(1, j) = f \, M_r(i_{max}, j - 1) \qquad [4]$$

Thus the total signal in the ith view of jth ventilatory cycle is given by

$$S(i, j) = [M_n(i, j) + M_r(i - 1, j)] \sin \alpha \qquad [5]$$

where the substitution in Eq. [4] is made at the beginning of each ventilatory cycle for M_r.

Figure 1 shows the theoretical signal (S) as a function of view number for a series of two respiratory cycles. We use the term signal in both the theory and experimental sections to indicate the integrated signal in a single view. The signal is measured experimentally by integrating the magnitude of the Fourier transform of that view. Because there is no recovery between views, the absolute time is irrelevant while the view number is most relevant. In this model, gas is infused during the first 20 views followed by continued RF excitations for an additional 30 views. The model shows two scenarios, the first with a limited excitation angle (α = 10 degrees) chosen to reduce the view-to-view variations, the second with a larger flip angle (α = 30 degrees) chosen to extract the maximum magnetization from each bolus.
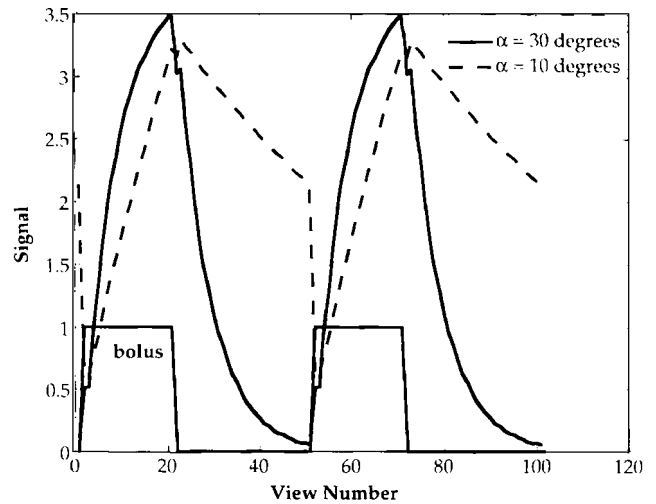

FIG. 1. Theoretical signal variation is shown as a function of view for two ventilatory cycles with α = 10 degrees and α 30 degrees.

METHODS

^{3}He gas was polarized using a procedure described in detail elsewhere (8, 9). A 50-cc Pyrex cell is charged to ~8 atmospheres with 2% N_2 and 98% ^{3}He. The cell contains a few milligrams of Rb metal. The cell is maintained at 170–180°C while it is illuminated with circularly polarized 7948 Å line from a 10-bar diode laser (Opto Power, Tucson, AZ), producing ~95 watts of usable optical power. The system yields about 350 cc of gas polarized to 5–10% in ~8 h.

Hyperpolarized gas is transferred to a 1000-cc plastic bag commonly used for intravenous fluid delivery. The bag is enclosed in a rigid sealed acrylic chamber. The rigid cylinder can be pressurized to control delivery of the gas from the more flexible bag. The acrylic chamber/bag is positioned 1 M from the end of the magnet bore, and the PE100 tubing, aligned parallel to the z axis of the magnet, connects the chamber to the breathing valve, which in turn connects directly to the endotracheal tube. The tidal volume of ^{3}He is controlled by regulated pressure applied to the chamber for the duration of inspiration. A two-stage, pneumatically controlled breathing valve made of Lexan controls both the breathing cycle (inspiration/expiration) and the switch between breathing air/isoflurane and ^{3}He (10). During proton imaging, the animal is ventilated normally with the air/anesthesia mixture. To maintain anesthesia and normal gas exchange during the short periods of helium imaging, the animal is alternately ventilated with air/anesthesia (about 3–5 cc tidal volume) and ^{3}He (1–2 cc tidal volume). For these studies, the duration of inspiration ranged from 200–300 ms, and expiration was 1200 ms. The expiratory valve was opened ~100 ms after the end of the ^{3}He infusion, and the gas was permitted to escape as the animal exhaled.

All animal procedures were approved by the Duke University Institutional Animal Care and Use Committee. Male guinea pigs (Harlan Sprague Dawley, Inc, Indianapolis, IN), ranging from 300–375 g, were anesthetized

with methohexital sodium (45 mg/kg, Brevital, Eli Lilly Co. Indianapolis, IN). A 3.5-cm long 14-gauge intracatheter (Sherwood Medical, Tullamore, Ireland) was inserted by tracheostomy and 3–0 silk ligatures were tied around the trachea to provide a gas-tight connection to the breathing valve. Thereafter, anesthesia was maintained with isoflurane (2.5–3.5%, Aerrane, Ohmeda Caribe Inc, Guayama, PR) delivered with a MRI-compatible ventilator using a custom-built breathing valve (see above) controlled pneumatically by computer (Macintosh, Apple Computer Inc, Cupertino, CA; TIO-10 digital board & LabVIEW 4.0 software, National Instruments, Austin, TX). The ventilator computer also supplied a trigger to the scanner co-incident with the beginning of He gas flow. ECG was recorded continuously from pediatric electrodes taped to the foot pads, a rectal thermistor monitored temperature, and a solid-state pressure transducer on the breathing valve monitored airway pressure. Physiologic signals were processed (Coulbourn Instruments, Allentown, PA) and displayed on a Macintosh computer using an A/D board (MIO-16, National Instruments) and LabVIEW software. A process-control feedback loop in the physiologic monitor software automatically controls body temperature by controlling the flow of heated air through the bore of the magnet.

Animals were imaged in a 7-cm diameter dual-frequency birdcage RF coil with one mode tuned to ^{1}H (85 MHz) and the orthogonal linear mode tuned to ^{3}He (63 MHz). Images were acquired in a 2.0 T, 30-cm bore magnet with shielded gradients (18 Gauss/cm). The system is controlled by a GE Signa console running Revision 5.4x software (GE Medical Systems, Milwaukee, WI).

Data were acquired using a projection encoding pulse sequence that has been developed explicitly for lung imaging [11]. Two-dimensional slice-selective and 3D non-slice-selective projection encoding is accomplished with multiple views per respiratory cycle. TR for these studies ranged from a minimum 3.7 to 10 ms, with up to 400 views acquired during each ^{3}He breath. The sequence was triggered directly from the ventilator. Projection encoding has four attributes that are particularly well suited to these studies:

1. The sequence is simple, allowing one to streamline the pulse sequence to run very rapidly.
2. It minimizes the consequences of diffusion; the effective echo time for these studies is <200 μs [12, 13].
3. It is much less sensitive to view-to-view variation from motion or other changes in the magnetization than Cartesian sampling strategies [14].
4. By summing the magnitude of the first few points in the FID, one has a direct measure of the magnetization in every view, enabling, in turn, the measurement of the temporal changes in the magnetization at temporal resolution of <4 ms.

To minimize the artifacts arising from view variation and to limit any periodicity from breath to breath, the angle of the radial views is randomized [15]. A fixed portion of the respiratory cycle is selected and views are acquired during this portion in random order with respect to view angle. The order is stored so that plots of

the magnetization versus view number (proportional to time) can be constructed retrospectively. All sorting and analysis was performed in MATLAB (The Math Works, Inc, Natick, MA).

RESULTS

Two-dimensional images were acquired in the coronal plane with the slice-selective gradients off in an effort to understand the relationship between the acquisition and flow effects. We hypothesized that if one acquired views during the early part of inspiration and used a large excitation angle, the resulting image would show primarily the larger bronchi. As the excitation angle is decreased, one might expect to see more and more of the lung anatomy, particularly the distal airways.

Figure 2 shows the changes in magnetization over two ventilatory cycles for four different acquisitions, each acquired with $TR = 10$ ms. Fifty views were acquired in each ventilatory cycle covering 500 ms of the total 1.5 s of each breath. Gas was infused for the first 200 ms, followed by a 300-ms period, during which the volume was held fixed, followed by a 1-s period for expiration. Data were acquired only for the breaths during which 2 cc of HP ^{3}He was infused. On the odd breaths, a 5-cc breath of 3% isoflurane in room air was supplied. Sixteen ^{3}He breaths (32 cc total) were supplied, with a total acquisition time of 48 s for each run, yielding 800 views for each data set. The four separate runs are identical except that the excitation angle is changed. The data plotted are from views acquired after the first five breaths of He, at which point an equilibrium of residual magnetization from previous breaths has been established. Using our earlier notation, we have plotted signal for $j = 6$, $i = 1$–50; $j = 7$, $i = 1$–50. For simplicity, we have numbered the views sequentially.

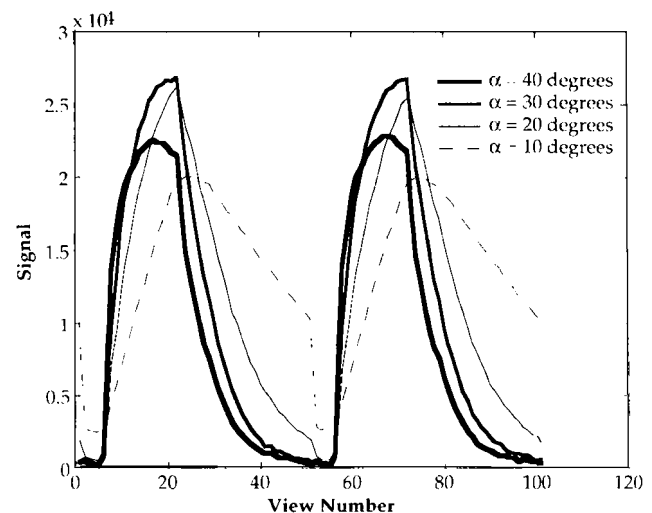The data are entirely consistent with our model. There is a gradual rise to an equilibrium magnetization (not

FIG. 2. Measured signal variation is shown as a function of view for two ventilatory cycles with $\alpha = 10$–40 degrees. The two cycles shown are ventilatory cycles 7 and 8, at which point the concentration of ^{3}He in the lung has reached an equilibrium.

shown) in the first few ventilatory cycles for $\alpha = 10$ and 20 degrees. We focus here on the variation of signal within a cycle. The response for all excitation angles is similar. The initial bolus results in a rapid rise in the signal to a maximum that then begins to decay as it is destroyed by the repetitive excitations. The slope on the leading edge of the input bolus is greater for the larger excitation angles because sin α is larger. The larger RF excitation destroys the magnetization more rapidly, which in turn weights these images with larger α to the earlier part of the ventilatory cycle. Conversely, a smaller α samples the magnetization further into the ventilatory cycle. The view-to-view variation is thus greatest for the larger angles and less prominent for smaller angles. There is one exception in this data at $\alpha = 40$ degrees: the signal does not reach as great a maximum as it does for $\alpha = 30$ and 20 degrees. This is attributable to a rapid destruction of the magnetization during the inflow. Note, for example, the shape of the rising part of the curve differs for $\alpha = 40$ degrees from that of the other smaller excitation angles. The signal begins to decline at approximate view 18–19, while it continues to grow for $\alpha = 10$–30 degrees, out to view 20–25. At this point, the magnetization is being destroyed as rapidly as it is replenished.

The view-to-view variation is the least for $\alpha = 10$ degrees. The magnetization at view 1 is $\sim 0.25 \times 10^4$, rising to a maximum of $\sim 2 \times 10^4$ at view 25, (i.e., a variation of $\sim 8:1$). A similar measure for $\alpha = 30$ degrees shows a view-to-view variation of greater than 20:1. The difficulty in the comparison comes from the fact that there is very little magnetization in the initial views for $\alpha = 20$–40 degrees. There is clearly residual magnetization in the initial views from the previous breath for $\alpha = 10$ degrees. The precipitous drop in signal at view 50 demonstrates that polarized gas is exhaled. There is a 2.5-s delay between view 50 and view 51 during which a 5-cc isoflurane/air breath is administered. This results in dilution of the residual signal as helium is flushed out, as well as some potential loss from T_1 decay in the lung. Note, however, that the signal does not decay to zero, indicating that some residual gas is retained in the end-expiratory volume of the lung.

Figure 3 shows the images constructed from these data. The images are also consistent with our model. Figure 3a shows the image acquired with $\alpha = 40$ degrees. As is clear from Fig. 2, the majority of the signal is sampled during the earlier phase of the inspiratory cycle and only larger airways are seen. As the angle is reduced, more of the magnetization is sampled later into the ventilatory cycle as it has traveled further into the lung. Figures 3b–3d show the effective distribution of the ^{3}He from the larger airways to the more distal airways. The ^{3}He, both polarized and unpolarized, reaches the distal spaces in all four cases. However, the point at which there is available signal has changed.

Significantly higher resolution images can be obtained using 3D projection encoding techniques (16). These acquisitions also permit one to follow the dynamics of the gas over much longer periods. Figure 4 shows a stacked plot from a 3D acquisition acquired with approximately 20,000 individual views. For each ventilatory cycle, the
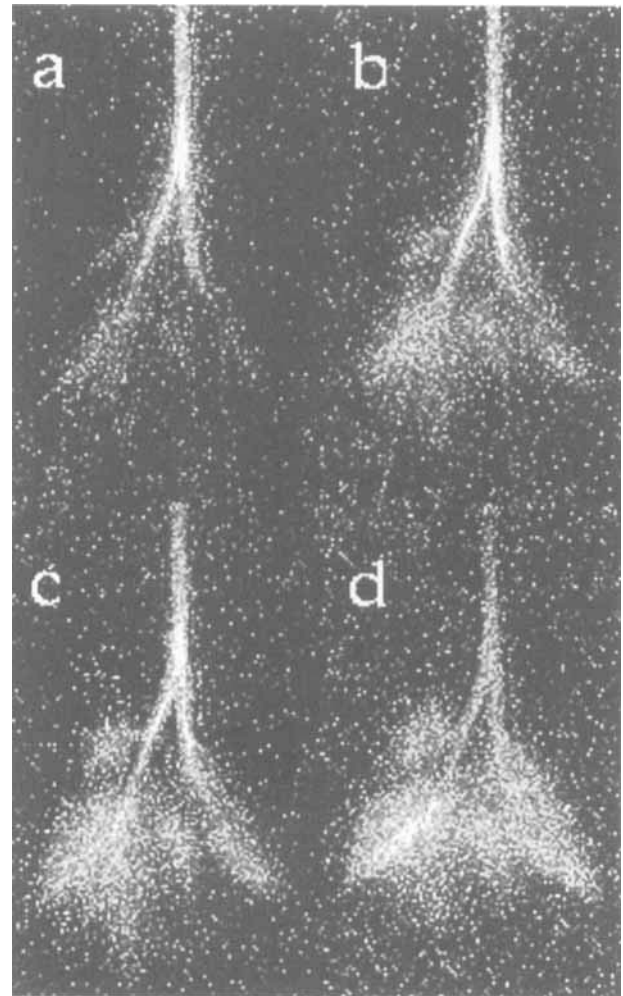

FIG. 3. Non-slice-selective coronal images of ^{3}He in a live guinea pig demonstrate presence of the gas in the more distal regions as α varies from (a) 40 degrees, (b) 30 degrees, (c) 20 degrees, to (d) 10 degrees.

bolus was infused during a 150-ms period as before, with an additional period of 150 ms at fixed volume, followed by a 1200-ms period during which the animal exhaled. Views were acquired in randomized fashion to fill an isotropic cube of k-space sufficient to reconstruct an $80 \times 80 \times 80$ element array with isotropic resolution of $0.5 \times 0.5 \times 0.5$ mm (0.125 mm^3). The repetition time was 3.7 ms, permitting acquisition of 400 views per ventilatory cycle. A total of 50 breaths (@ 2 cc/breath, i.e., 100 cc of ^{3}He) was administered on alternate ventilatory cycles, requiring a total acquisition time of 2.5 min. The excitation angle was 6 degrees, resulting in data acquisition over roughly half of each ventilatory cycle. A pressure transducer was mounted on the breathing valve. The pressure at that point is plotted along with the digital pulses used to trigger both the expiratory and inspiratory valves.

The stacked plot with temporal sampling of 3.7 ms in Fig. 4 allows us to examine the dynamics of the magnetization in much greater detail. The signal during the time t_0–t_1 is probably due to residual magnetization from previous views and gas in the valve forced into the air-
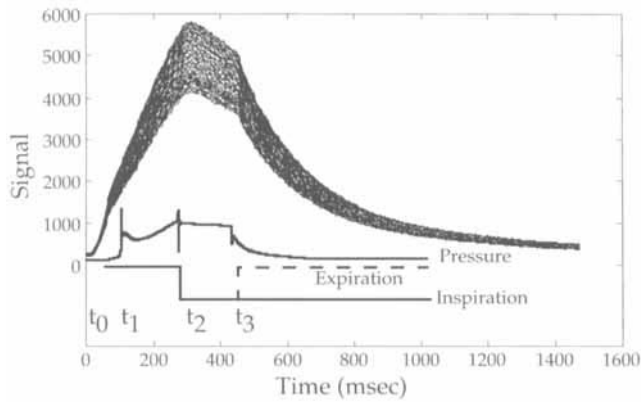
FIG. 4. The stacked plot shows signal variation in multiple ventilatory cycles of a 3D acquisition in a live guinea pig. The signal rises rapidly during t_1–t_2 as the gas flows in. The signal decays approximately linearly from t_2–t_3 as the animal is maintained at a fixed volume. The signal decays more rapidly after t_3 as the animal exhales.

way before registration of any pressure change in the transducer. At t_1, the pressure begins to rise. The signal rises almost linearly until time t_2, at which point the inspiratory valve closes, shutting off the supply of gas. "Held breath" occurs from t_2 to t_3. During this period, the pressure is reasonably constant and the signal decays almost linearly because the excitation angle is small. At t_3, the expiratory valve opens and the gas is exhaled. From t_3 until the end of the acquisition, the signal decays in a nonlinear fashion as magnetization continues to be destroyed by the closely spaced RF pulse and while gas is gradually exhaled. Over the 2.5-min course of the study, the peak signal in each ventilatory cycle decays from an initial value of ~6000 to ~4000 in the last cycle. We attribute this to T_1 losses in the external reservoir from which the gas is administered.

Figure 5 shows representative images from an isotropic 3D image array acquired in a fashion similar to those in Fig. 4. The data were acquired with a limited flip angle (α = 12 degrees) and a smaller volume of gas in each bolus (1.5 cc), allowing acquisition of sufficient data to reconstruct an isotropic 128^3 array with spatial resolution of $0.5 \times 0.5 \times 0.5$ mm (0.125 mm^3). Fifty-one thousand four hundred views were acquired with 128 breaths (each 1.5 s), with a total acquisition time of 6.4 min. Figure 5a shows a coronal projection of the entire volume. The main stem bronchi and several branching airways are clearly seen. The 3D images are displayed using a ray tracing algorithm where the final projected image is a consequence of the entire path used in the ray tracing algorithm. A 7.5-mm subvolume has been selected from the entire 3D array for display in Fig. 5b. By removing the overlying structures, branching airways to the fourth order are clearly visible. Because the data are isotropic, it is straightforward to render through any plane without loss of spatial resolution. Figure 5c shows a single 0.5-mm axial slice in the center of the slab indicated in Fig. 5b. Figure 5c shows the entire volume-rendered axial slab. The relatively low flip angle and requirement that we obtain data over a large segment of the ventilatory cycle results in significant signal in the more distal areas.

While the spatial resolution is not yet sufficient to resolve the alveoli, the background signal in the parenchymal air spaces serves to highlight the blood vessels (black) in which there is no signal. Note the presence of the brighter airway filled with gas immediately adjacent to the blood vessels. With some attention to the volume rendering parameters, it is possible in Fig. 5d to render images in which airways at least to the fourth level of branching are visible.

CONCLUSIONS

Steady improvements in the physics of HP gas production have resulted in a compact system capable of routine production of 300 cc of gas polarized to 5–10% in ~8 h. The reliable operation of the unit has permitted us to undertake a systematic study of the dynamic behavior of polarized gas during an imaging study. Projection encoding has been developed to simultaneously address the problems of diffusion and view variation while providing an easy method to measure the changes in polarization at temporal sampling of <4 ms. An iterative model of the polarization dynamics has been constructed that includes dilution effects of the input bolus and loss of polarization from exhaled gas. Agreement between the model and experiment is excellent.
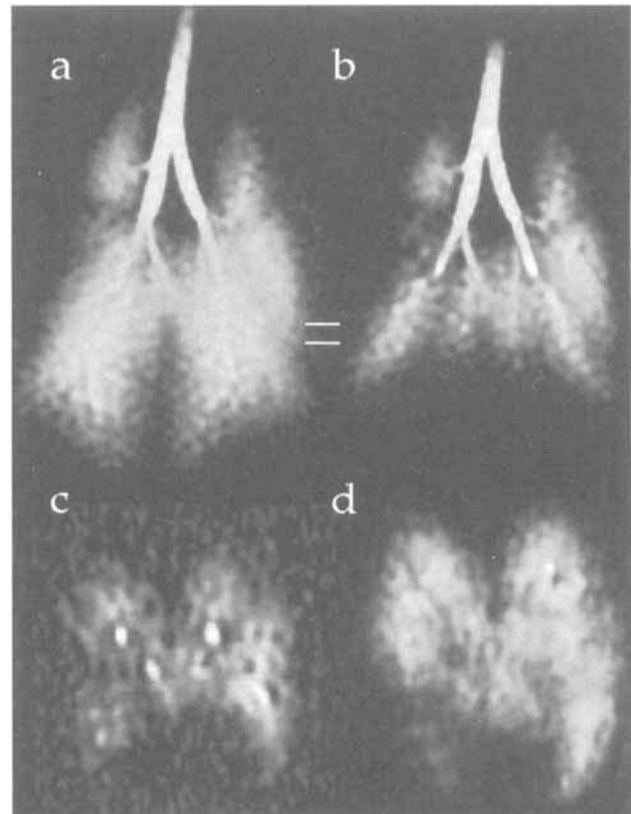

FIG. 5. Selected views have been volume rendered from a 128^3 isotropic array acquired in 6.4 min: (a) a coronal view of the entire volume, (b) a 7.5-mm coronal slab showing airways down to the fourth order, (c) the central axial slice from the slab marked in (a), and (d) the axial slab, in which vessels appear as signal voids.

The signal from polarized gas varied by as much as a factor of 20 through a single ventilatory cycle. The consequences of this view-to-variation will have significant impact on the choice of imaging strategies, e.g., projection acquisition versus conventional spin warp. The total variation is directly dependent on the flip angle and TR chosen. Flow effects are clearly measurable in saturation studies where a larger flip angle results in rapid depolarization in the early part of the ventilatory cycle, in turn yielding images primarily of the larger airways.

The T_1 of the gas in the supply reservoir and speed of the 3D projection encoding scheme are such that 3D images with volume resolution of 0.125 mm^3 can be obtained in ~6 min. T_1 of the gas in the high pressure reservoir of the polarizer is typically 6–8 h. This long T_1 is crucial to the polarizing process and it is obtained through careful cleaning and preparation of the cell. T_1 in the holding reservoir has been estimated by looking at the decay of the peak amplitude of the magnetization during individual respiratory cycles through the course of the 3D acquisition. The T_1 in the reservoir is ~30 min. But very little effort has been made to prepare this reservoir so one might reasonably expect considerably longer holding periods. This, of course, would support longer acquisition periods, which would be particularly useful for MR microscopy in small animals.

The model developed here allows us to select a flip angle to make the greatest use of the polarization in a given bolus, minimizing losses from exhaled gas while sampling through any given part of the ventilatory cycle. The combination of improved SNR and spatial resolution permit definition of the smallest anatomical structures yet seen in HP gas MRI with clear definition of the conducting airways down to at least the 4th order and definition of major blood vessels.

These early results in HP MRI are encouraging. Initial concerns of problems from diffusion seem to be of less significance as airways less than 1 mm in diameter are clearly visible. A clearer understanding of the dynamics of polarized gas will allow us to design better imaging strategies for both higher temporal and spatial resolution. The distinctive properties of HP MRI (e.g., significant increase in SNR and operation in a nonequilibrium setting) pose new challenges and opportunities for creative imaging strategies. There seems little doubt that HP MRI will yield significant benefit in characterizing the lung for both the basic scientist and the clinician.

REFERENCES

1. H. Middleton, R. Black, B. Saam, G. Cates, G. Cofer, B. Guenther, W. Happer, L. Hedlund, G. Johnson, K. Juvan, J. Swartz, MR imaging with hyperpolarized He-3 gas. *Magn. Reson. Med.* **33**, 271–275 (1995).
2. G. Johnson, G. Cofer, R. Guenther, W. Happer, L. Hedlund, H. Middleton, J. Swartz, MRI using hyperpolarized gas, *in* "Proc., SMR, 3rd Scientific Meeting, Nice, France, 1995," p. 392.
3. R. Black, H. Middleton, G. Cates, G. Cofer, B. Driehuys, W. Happer, L. Hedlund, G. Johnson, M. Shattuck, J. Swartz, In vivo He-3 MR images of guinea pig lungs. *Radiology* **199**, 867–870 (1996).
4. J. MacFall, H. Charles, R. Black, H. Middleton, J. Swartz, B. Saam, B. Driehuys, C. Erickson, W. Happer, G. Cates, G. Johnson, C. Ravin, Human lung air spaces: potential for MR imaging with hyperpolarized He-3. *Radiology* **200**, 553–558 (1996).
5. P. Bachert, L. R. Schad, M. Bock, M. V. Knoop, M. Ebert, T. Grossman, W. Heil, D. Hofmann, R. Surkau, E. W. Otten. Nuclear magnetic resonance imaging of airways in humans with use of hyperpolarized ^{3}He. *Magn. Reson. Med.* **36**, 192–196 (1996).
6. M. Wagshul, T. M. Button, H. F. Li, Z. Liang, C. S. Springer, K. Zhong, A. Wisnia, In vivo MR imaging and spectroscopy using hyperpolarized ^{129}Xe. *Magn. Reson. Med.* **36**, 183–191 (1996).
7. K. Sakai, A. M. Bilek, E. Oteiza, R. L. Walsworth, D. Balamore, F. A. Jolesz, M. S. Albert, Temporal dynamics of hyperpolarized ^{129}Xe resonance in living rats. *J. Magn. Reson. Series B* **111**, 300–304 (1996).
8. M. Bouchiat, T. Carver, C. Varnum, Nuclear polarization in ^{3}He gas induced by optical pumping and dipolar spin exchange. *Phys. Rev. Lett.* **5**, 373–377 (1960).
9. T. Chupp, M. Wagshul, K. Coulter, A. McDonald, W. Happer, Polarized high-density gaseous ^{3}He targets. *Phys. Rev. C* **36**, 2244–2251 (1987).
10. L. Hedlund, M. Shattuck, G. Johnson, Three-dimensional MR microscopy of pulmonary dynamics, *in* "Proc., SMR, 4th Scientific Meeting, New York, 1996," p. 327.
11. M. Shattuck, G. Cofer, G. Glover, L. Hedlund, G. Johnson, Three-dimensional projection microscopy of the lung, *in* "Proc., SMR 4th Scientific Meeting, New York, 1996," p. 18.
12. P. C. Lauterbur, C. M. Lai, Zeugmatography by reconstruction from projections. *IEEE Trans. Nucl. Sci.* **NS-27**, 1227–1231 (1980).
13. P. T. Callaghan, C. D. Eccles, Diffusion-limited resolution in nuclear magnetic resonance microscopy. *J. Magn. Reson.* **78**, 1–8 (1988).
14. G. Glover, J. Pauly, Projection reconstruction techniques for reduction of motion effects in MRI. *Magn. Reson. Med.* **28**, 275–289 (1992).
15. G. Glover, D. Noll, Consistent projection reconstruction (CPR) techniques for MRI. *Magn. Reson. Med.* **29**, 345–351 (1993).
16. C. M. Lai, P. C. Lauterbur, True three-dimensional image reconstruction by nuclear magnetic resonance zeugmatography. *Phys. Med. Biol.* **26**, 851–856 (1981).